

# The Search for Predictable Features of Relativistic Electron Events: Results from the GEM Storms Campaign

G. D. REEVES, K. L. MCADAMS, R. H. W. FRIEDEL, AND T. E. CAYTON

*Los Alamos National Laboratory, Los Alamos, New Mexico 87545*

We have examined the relativistic electron events associated with four geomagnetic storms driven by CME-produced magnetic clouds in order to discover some of the underlying consistent behavior that is common to these events. The geomagnetic conditions for the four events showed considerable variation as did the fluxes at fixed energies and fixed L-shell. By combining data from nine different satellites and by selecting specific parameters we found several characteristics of the relativistic electron events that were consistent from storm to storm. Our analysis focused on geosynchronous orbit and on  $L \approx 4.2$  which is near the heart of the outer electron belt. We examined a large number of parameters and combinations of parameters and found that among the most consistent sets were (1) the temporal behavior of the electron fluxes at  $L \approx 4.2$  and  $L \approx 6.6$ , (2) the temporal evolution of the spectra at  $L \approx 4.2$  and  $L \approx 6.6$ , and (3) the gradients of the phase space densities between  $L \approx 4.2$  and  $L \approx 6.6$ . The characteristics of those parameters may be common to all relativistic electron events and if so that they hold important clues to the physical processes operating during these events. The fact that they are common to these four storms already provides an important framework for evaluating the success of various predictive space weather models that are being developed and tested against these four events.

## 1. INTRODUCTION

A common feature of geomagnetic storms, and one with important space weather implications, is the enhancement of electrons with relativistic energies in the Earth's outer radiation belts. Electrons with sufficiently high energies can penetrate spacecraft and instrument shielding causing damage to materials and circuits. The amount of energy required depends on the type and thickness of the shielding but most studies consider electrons with energies greater than 2 MeV which will penetrate approximately 300 mils of aluminum.

Relativistic electrons can cause damage in a number of ways but the most common concerns are damage to materials through total radiation dose and damage to electronics through deep dielectric charging (also referred to as bulk charging). When electrons penetrate the protective layer of shielding they will impact other materials. If those materials are insulators then charge will become embedded in the material. If the rate of charge deposition is higher than the rate of charge leakage, then bulk charge will build up and will eventually discharge. The results can be minor, such as

spurious signals in coaxial cables, or dramatic, such as the failure of critical electrical components. Deep dielectric charging from relativistic electron enhancements is a well-known hazard that is typically mitigated through prudent spacecraft design. Nevertheless, the risk is probabilistic and difficult to quantify, even in very cautious designs, and a number of serious spacecraft failures have been at least circumstantially linked to enhanced relativistic electron fluxes [Baker *et al.*, 1998].

The risk of deep dielectric charging is proportional to the flux of relativistic electrons and to the hardness of the spectrum. Both are known to vary on a wide range of time scales ranging from minutes to a solar cycle. Relativistic electron enhancements are most commonly observed in the approach to solar minimum when high-speed solar wind streams from coronal holes buffet the Earth's magnetosphere. In fact the strong correlation between solar wind velocity and relativistic electron fluxes remains one of the best predictors of relativistic electron events [Paulikas & Blake, 1979; Baker *et al.*, 1990; Belian *et al.*, 1996]. When coronal holes are particularly long-lived, periodic enhancements of the

relativistic electron fluxes can be observed every Carrington rotation – sometimes for over half a year.

If coronal holes were the only solar driver for relativistic electron events we would have a firm basis for predictions, but they are not. Relativistic electron events are also commonly caused by more random and impulsive solar activity. Blake *et al.*, [1992] and Li *et al.*, [1993] have documented the extremely sudden (several minute) enhancement of relativistic electrons to energies greater than 25 MeV by the passage of an interplanetary shock in March 1991. Relativistic electron enhancements are also commonly observed in association with Coronal Mass Ejections (CMEs) with and without associated shocks [e.g. Baker *et al.*, 1998; Knip *et al.*, 1998; Reeves *et al.*, 1998a].

While there is a good association between solar wind drivers and the relativistic electron response the relationship is not quantitatively predictable. Not all CMEs produce relativistic electron enhancements. Likewise Paulikas & Blake's [1979] plot of solar wind velocity vs. relativistic electron flux showed significant scatter until 27-day averages were taken. Blake *et al.*, [1997] suggested that the amount of southward IMF Bz might play a role in producing a "seed population" of  $\approx 100$  keV electrons for subsequent acceleration. However, southward IMF Bz and high solar wind velocity are exactly the ingredients necessary for building up the storm-time ring current but Reeves [1998] showed that while 90% of geomagnetic storms in 1994 were accompanied by relativistic electron enhancements the correlation between their peak amplitudes was less than about 60%.

Because there is considerable variety in the solar wind conditions that drive relativistic electron enhancements there is also considerable variety from event to event. This can sometimes make the job of modeling a particular event in all its particulars seem rather daunting. In this study we take a different approach which is to try to determine the fundamental underlying conditions that are common among several events in order to provide a baseline for predictive models and for greater physical understanding.

## 2. THE GEM CAMPAIGN STORMS

The Geospace Environment Modeling (GEM) program is sponsored by the US National Science Foundation and has as one of its goals, improved observational, theoretical, and predictive understanding of the dynamics of the inner magnetosphere during geomagnetic storms. To this end the GEM Inner Magnetosphere/Storms campaign selected three geomagnetic storms for intensive study. These storms took place in May 1997, September 1998, and October 1998. In this study we also compare the January 1997 storm which has been extensively documented in the scientific literature [e.g. Reeves *et al.*, 1998a].

Figure 1 shows the geophysical conditions for each of these four events. From top to bottom, the panels show the Dst index, the Kp index, the IMF Bz component, the solar wind ion density, and the solar wind velocity. For the four storms the minimum Dst ranged from -85 to -228 and maximum solar wind velocity ranged from 500 km/s in May 1997 to 930 km/s in September 1998 while the other parameters also showed considerable variation. All four storms in this study were driven by CME-produced magnetic clouds.

Figure 2 shows the relativistic electron fluxes throughout the outer radiation belts for the four storms. These plots show the flux of electrons with energies greater than approximately 2 MeV as a function of L-shell with a 3-hour time resolution. The high time-resolution for these events, which is essential for resolving the storm-time dynamics, was obtained by combining the data from nine separate satellites: POLAR, GOES-8, GOES-9, GPS NS-24, GPS NS-33, 1990-095, 1991-080, 1994-084, and SAMPEX [McAdams *et al.*, 2000]. Figure 2 shows that both the intensity and the temporal behavior of the  $>2$  MeV electron fluxes varies from event to event. Although it is not shown in the figure, those differences are apparent at all measured energies.

By combining data from a large number of satellites we can essentially specify the relativistic electron fluxes as a function of time, energy, L-shell, and local time to produce what is essentially a "data synthesis model" for each event [e.g. Reeves *et al.*, 1998b]. These models are extremely useful for detailed analysis of a particular event and how it may have affected a particular satellite which may or may not have been equipped with environmental monitoring instruments. However, production of these data synthesis models is labor intensive and does not, by itself, provide any physical insight into the acceleration and transport processes.

## 3. COMMON ELEMENTS OF THE GEM STORMS

Using the specification of the four storms provided by all nine satellites we searched for common elements of the storms which could provide a basis for inter-comparison and for developing physical models. We examined a large number of parameters and combinations of parameters and found that among the most consistent sets were (1) the temporal behavior of the electron fluxes at  $L \approx 4.2$  and  $L \approx 6.6$ , (2) the temporal evolution of the spectra at  $L \approx 4.2$  and  $L \approx 6.6$ , and (3) the gradients of the phase space densities between  $L \approx 4.2$  and  $L \approx 6.6$ .

### 3.1 Temporal Behavior of Fluxes at $L \approx 4.2$ vs. $L \approx 6.6$

A useful rule of thumb for spacecraft operators has been that the relativistic electron fluxes peak 3-4 days after the onset of a geomagnetic storm. This time delay

was thought to provide ample lead time for any needed change in operations. The time delay was also one of the primary observational motivations for the proposition that a slow “recirculation” process was responsible for the relativistic electron acceleration [Nishida 1976; Fujimoto & Nishida 1990].

One of the interesting observations from study of the January 1997 storm was that the relativistic electron fluxes at  $L \approx 4.2$  increased much more quickly, reaching a peak within 12 hours after they began to rise. Reeves et al., [1998a] concluded that the acceleration of the relativistic electrons in the heart of the radiation belts was relatively rapid (less than 1 day) and that the peak observed 3-4 days following the storm onset was a characteristic primarily of the outer edge of the trapping region which includes  $L \approx 6.6$ . They attributed the delay at geosynchronous orbit to a redistribution of particles in the magnetosphere – perhaps outward radial diffusion.

We see from Figure 3 that this behavior is indeed common to all four storms. In each event there is an initial decrease in the relativistic electron fluxes which is attributable to an adiabatic response to the ring current – the so-called Dst effect [Kim & Chan, 1997]. Following the dip there is a very rapid increase in the fluxes measured at  $L \approx 4.2$ . In all cases the rise to maximum at  $L \approx 4.2$  is on the order of a half a day. After reaching maximum levels the fluxes at  $L \approx 4.2$  remain nearly constant or decrease slightly. The October 1998 storm is different in two respects. As with the other storms the fluxes at  $L \approx 4.2$  increase rapidly following the main-phase Dst decrease but they also continue to rise slowly over the following several days. Careful examination of the L-shell profiles show that this is because the radial position of the flux peak (in L) moved outward in time during the October storm causing the fluxes at the fixed position of  $L \approx 4.2$  to increase. We suspect that this may be related to the continued activity reflected in the Kp index (Figure 1).

The other difference is that the  $>2$  MeV electron fluxes were already elevated before the storm so this event did not produce an overall increase in the fluxes at  $L \approx 4.2$ . In fact, we note that new activity can actually produce a sustained decrease in the relativistic electron fluxes even at  $L \approx 4.2$ . This is seen, for example, on Day 274 of the September 1998 event when a new interval of moderate activity (IMF Bz south,  $Kp > 4$ , and  $Dst < -85$  nT) appeared to “reset” the fluxes at  $L \approx 4.2$  to a lower level.

### 3.2 Spectral Behavior at $L \approx 4.2$ vs. $L \approx 6.6$

While the temporal evolution of the fluxes at  $L \approx 4.2$  and  $L \approx 6.6$  exhibit some important common characteristics the precise nature of those characteristics is a function of energy and fluxes at different energies can appear to exhibit quite different temporal behavior.

However, when one examines the characteristics of the spectra themselves a satisfying consistency emerges.

McAdams et al., [2000] fit the fluxes measured by GPS at  $L \approx 4.2$  and the fluxes measured by the LANL geosynchronous satellites at  $L \approx 6.6$  to a simple exponential,

$j(E) = C \exp(-E/E_0)$ . Figure 4 shows the temporal profiles of  $C$ , which is the number of electrons with energy greater than 200 keV (a “density”) and  $E_0$ , which is the spectral slope (or “temperature”).

One interesting feature is that  $C$  and  $E_0$  change much more abruptly than the  $>2$  MeV fluxes. On this time scale the change appears nearly instantaneous. (When no points are plotted the fluxes are too low to obtain a meaningful spectral fit.)

Subsequent to the sudden change in spectrum the “density” begins to decrease at both L-shells ( $C$  decreases) and the spectrum at  $L \approx 4.2$  gets harder ( $E_0$  increases). The changes at  $L \approx 4.2$  are consistent with a sudden “injection” of particles and a subsequent loss of the low-energy component of the spectrum (probably due to pitch angle scattering). At geosynchronous orbit the increase in “density” is nearly simultaneous with that seen at  $L \approx 4.2$  and the decrease over time is at roughly the same rate (with some interesting differences). The spectral slope at geosynchronous seems to stay roughly constant. It actually peaks and decreases roughly in concert with the  $>2$  MeV fluxes but the changes are small compared to the changes at  $L \approx 4.2$ .

### 3.3 Phase Space Densities at $L \approx 4.2$ vs. $L \approx 6.6$

Theoretical studies and physical models of the relativistic electron belts are almost always cast in terms of phase space densities at fixed values of the adiabatic invariants while spacecraft observations are almost always at fixed energies. Closer connection between the models and observations can be obtained if measured fluxes can be converted to phase space density. This can be done if certain assumptions are made. Here we restrict our analysis to locations where the satellites are near the magnetic equator (geosynchronous and  $L \approx 4.2$  for GPS). We use a model magnetic field to calculate the first invariant, we assume that the second invariant is strictly zero (e.g.  $90^\circ$  pitch angles), and we assume that the magnetic field is time stationary [McAdams et al., 2000]

The resulting phase space densities for five values of  $\mu$ , the first invariant, are plotted in Figure 5. The range of  $\mu$  corresponds to electron energies of 100 keV to 1.4 MeV at geosynchronous and 320 keV to 3.1 MeV at  $L \approx 4.2$ . And, we use the spectral fits shown in Figure 4 to derive the fluxes used to calculate the phase space densities at appropriate values of  $\mu$ .

Several interesting and consistent features are apparent in the phase space density profiles. First we note that for the range of  $\mu$  values plotted, and for all four storms, the phase space densities at  $L \approx 6.6$  are

always greater than those at  $L \approx 4.2$  indicating that there is a sufficiently large source population at high L-shells that diffusive transport is a viable mechanism.

Second, we find that there are distinct differences at high and low values of  $\mu$  – particularly at  $L \approx 4.2$ . At low  $\mu$  the phase space density decreases in the ten days following the storm, which is indicative of the loss of low-energy particles through pitch angle scattering. Interestingly, at low values of  $\mu$  the gradient in phase space density remains nearly constant over this relatively long time period.

Instead of decreasing over time, the phase space densities at higher  $\mu$  for  $L \approx 4.2$  systematically increase over time. At  $L \approx 6.6$  the phase space densities do not show as big a difference with increasing  $\mu$  as they do at  $L \approx 4.2$  although they can also show a gradual increase for some period of time. In the several days following the storm, though, the gradients at high  $\mu$  decrease until, after about ten days the phase space densities are nearly equal.

While the physical processes responsible for these phase space density profiles are still a matter of current research, it is clear that there is a degree of consistency among these four storms which any successful model of relativistic electron events would need to reproduce.

#### 4. CONCLUSIONS

We have examined the relativistic electron events associated with four geomagnetic storms driven by CME-produced magnetic clouds in order to discover some of the underlying consistent behavior that is common to these events. The geomagnetic conditions for the four events showed considerable variation. The Dst index ranged from -85 to -228 nT and maximum solar wind velocity ranged from 500 km/s to 930 km/s. When plotted as fluxes at fixed energies and fixed L-shells the relativistic electron response in the outer radiation belts also varies considerably from storm to storm.

By combining data from nine different satellites and by selecting specific parameters we found several characteristics of the relativistic electron events that were consistent from storm to storm. Our analysis focused on geosynchronous orbit and on  $L \approx 4.2$  which is near the heart of the outer electron belt and, importantly, where the GPS satellites cross the magnetic equator.

We found that the fluxes of  $>2$  MeV electrons at  $L \approx 4.2$  and  $L \approx 6.6$  for the three GEM storms were quite similar to the behavior described by Reeves et al., [1998a] for the January 1997 storm. The  $>2$  MeV fluxes at  $L \approx 4.2$  increase quite rapidly (on the order of 12 hours) and then remain nearly constant over the next ten days. The well-known 3-4 day delay between storm onset and peak relativistic electron fluxes appears to be characteristic of the outer edges of the electron belts, near geosynchronous orbit.

The relativistic electron spectra also had common characteristics among the four storms. The change in spectra at both L-shells was even more abrupt than the change in fluxes. In particular the “density” of electrons with energies above 200 keV increase sharply and then decrease monotonically over time. The rate of decrease at  $L \approx 4.2$  and  $L \approx 6.6$  was nearly the same. Although the spectral slope at  $L \approx 6.6$  changes over time the changes are small compared to those at  $L \approx 4.2$  and do not show the same consistent hardening over time.

We also used the spectral fits and an assumed magnetic field to calculate phase space densities which also showed a more consistent behavior than the fluxes at fixed energy. We found that for all values of  $\mu$  considered here the phase space densities at geosynchronous were higher than at  $L \approx 4.2$  but that the gradient decreased with increasing  $\mu$ . At  $L \approx 4.2$  we found that the phase space densities at low  $\mu$  decreased slowly over time while at high  $\mu$  they increased. The differences between low and high  $\mu$  at  $L \approx 6.6$  were not as strong so, while at low  $\mu$  the phase space density gradient remained nearly constant, at high  $\mu$  the gradient decreased over time and nearly disappeared after ten days.

We suspect that these features may be common to all relativistic electron events and if so that they hold important clues to the physical processes operating during these events. The fact that they are common to these four storms already provides an important framework for evaluating the success of various predictive space weather models that are being developed and tested against these events.

*Acknowledgments.* We would like to thank R. D. Belian, R. A. Christensen, S. Kanekal, J. B. Blake, R. Selesnick, W. C. Feldman, and J. F. Fennell for their help in acquiring and processing the data used in this study. We also thank the US Department of Energy Office of Basic Energy Science (OBES) for support of this study.

#### 5. REFERENCES

- Baker, D. N., R. L. McPherron, T. E. Cayton, and R. W. Klebesadel, Linear prediction filter analysis of relativistic electron properties at 6.6  $R_E$ , *J. Geophys. Res.*, **95**, 15,133, 1990.
- Baker, D. N., T. Pulkkinen, X. Li, S. G. Kanekal, J. B. Blake, R. S. Selesnick, M. G. Henderson, G. D. Reeves, H. E. Spence, and G. Rostoker, Coronal mass ejections, magnetic clouds, and relativistic magnetospheric electron events: ISTP, *J. Geophys. Res.*, **103**, 17,279, 1998.
- Belian, R. D., T. E. Cayton, R. A. Christensen, J. C. Ingraham, M. M. Meier, G. D. Reeves, and A. J. Lazarus, Relativistic electrons in the outer-zone: An 11-year cycle; their relation to the solar wind, in *Workshop on the Earth's Trapped Particle Environment*, edited by G. D. Reeves, AIP Press, New York, 13-18, 1996.

- Blake, J. B., D. N. Baker, N. Turner, K. W. Ogilvie, and R. P. Lepping, Correlation of changes in the outer-zone relativistic electron population with upstream solar wind and magnetic field measurements, *Geophys. Res. Lett.*, **24**, 927-929, 1997.
- Blake, J. B., W. A. Kolasinski, R. W. Fillius, and E. G. Mullen, Injection of electrons and protons with energies of tens of MeV into  $L < 3$  on 24 March 1991., *Geophys. Res. Lett.*, **19**, 821, 1992.
- Fujimoto, M., and A. Nishida, Energization and isotropization of energetic electrons in the Earth's radiation belt by the recirculation process, *J. Geophys. Res.*, **95**, 4625, 1990.
- Kim, H.-J., and A. A. Chan, Fully-adiabatic changes in storm-time relativistic electron fluxes, *J. Geophys. Res.*, **102**, 22,107-22,116, 1997.
- Knipp, D. J., N. Crooker, M. Engebretson, X. Li, A. H. McAllister, T. Mukai, S. Kokubun, G. D. Reeves, T. Obara, A. Weatherwax, and B. A. Emery, An overview of the early November 1993 geomagnetic storm, *J. Geophys. Res.*, **103**, 26,197-26,220, 1998.
- Li, X., R. Roth, M. Temerin, J. R. Wygant, M. K. Hudson, and J. B. Blake, Simulation of the prompt energization and transport of radiation belt particles during the March 24, 1991, SSC, *Geophys. Res. Lett.*, **20**, 2423, 1993.
- McAdams, K. L., G. D. Reeves, R. H. W. Friedel, and T. E. Cayton, Multisatellite comparisons of the radiation belt response to the GEM magnetic storms, *J. Geophys. Res.*, *submitted*, 2000.
- Nishida, A., Outward diffusion of energetic particles from the Jovian radiation belt, *J. Geophys. Res.*, **81**, 1771, 1976.
- Paulikas, G. A., and J. B. Blake, Effects of the solar wind on magnetospheric dynamics: Energetic electrons at the synchronous orbit, in Quantitative Modeling of Magnetospheric Processes, Geophys. Monogr., Amer. Geophys. Un., **21**, 180, 1979.
- Reeves, G. D., D. N. Baker, R. D. Belian, J. B. Blake, T. E. Cayton, J. F. Fennell, R. H. W. Friedel, M. G. Henderson, S. Kanekal, X. Li, M. M. Meier, T. Onsager, R. S. Selesnick, and H. E. Spence, The Global Response of Relativistic Radiation Belt Electrons to the January 1997 Magnetic Cloud, *Geophys. Res. Lett.*, **17**, 3265-3268, 1998a.
- Reeves, G. D., R. H. W. Friedel, and R. Hayes, Maps could provide space weather forecasts for the inner magnetosphere, *EOS Trans. AGU*, **79**, 613, 1998b.
- Reeves, G. D., Relativistic electrons and magnetic storms: 1992-1995, *Geophys. Res. Lett.*, **25**, 1817, 1998.

---

G. D. Reeves, K. L. McAdams, R. H. W. Friedel, and T. E. Cayton, Mail Stop D-466, NIS-1, Los Alamos National Laboratory, Los Alamos, NM 87545, USA (email: reeves@lanl.gov)

## FIGURE CAPTIONS

**Figure 1.** Geophysical conditions for the four storms. For each event we plot, from top to bottom, the Dst index, the Kp index, the IMF Bz component, the solar wind density, and the solar wind velocity.

**Figure 2.** The flux of  $>2$  MeV electrons as a function of time and L-shell. The color scale ranges in  $\log(\text{flux})$  from 2 (black) to 6 (red). The Dst index for each event is shown below for reference.

**Figure 3.** The flux of  $>2$  MeV electrons measured near  $L=4.2$  near the heart of the outer electron belt and at  $L=6.6$ , geosynchronous orbit. The fluxes measured by each satellite are color coded by spacecraft.

**Figure 4.** Parameters of an exponential fit to the spectra measured at  $L\approx 4.2$  (red) and  $L\approx 6.6$  (blues).  $C$  represents the “density” of electrons above 200 keV and  $E_0$  is the spectral slope or “hardness”.

**Figure 5.** The phase space densities measured at  $L\approx 4.2$  (red) and  $L\approx 6.6$  (blues) at fixed values of the adiabatic invariants. For each event we plot phase space densities for five different values of the first invariant,  $\mu$ , ranging from 100 to 3000 MeV/nT which corresponds to an energy range of 100 keV to 1.4 MeV at  $L=6.6$  and 320 keV to 3.1 MeV at  $L=4.2$ .

Short Title:

PREDICTABLE FEATURES OF RELATIVISTIC ELECTRON EVENTS: RESULTS FROM THE GEM CAMPAIGN

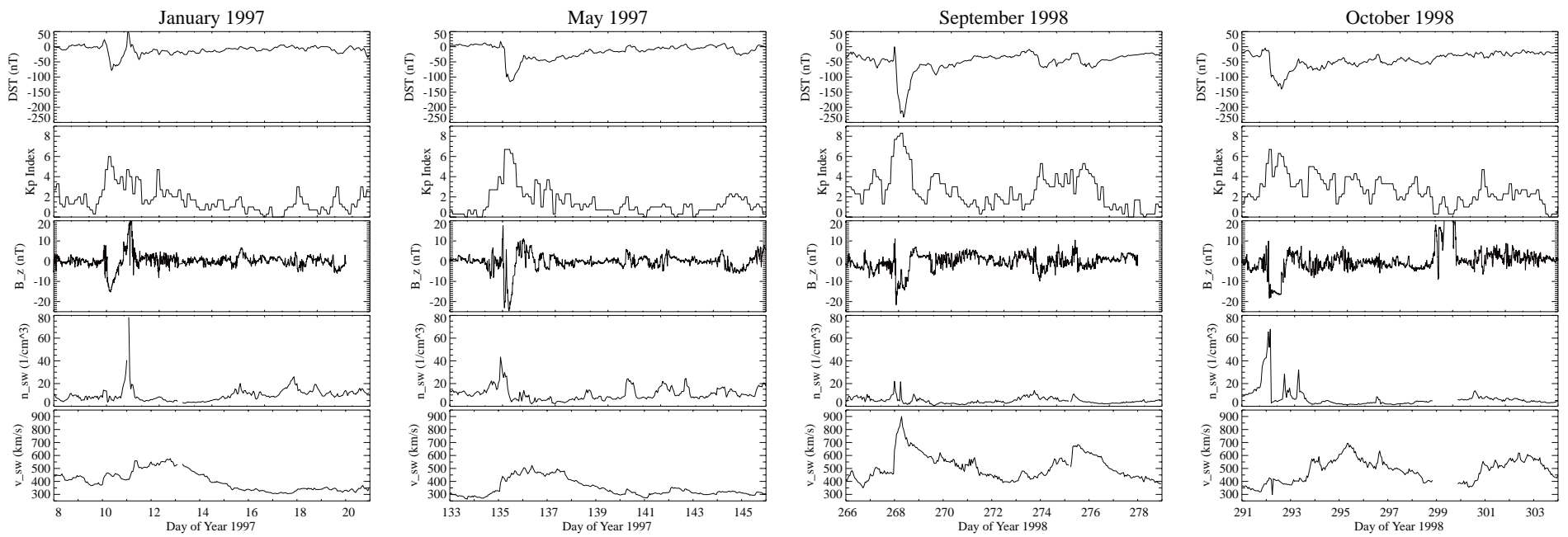


Figure 1  
2-column, print at 66%

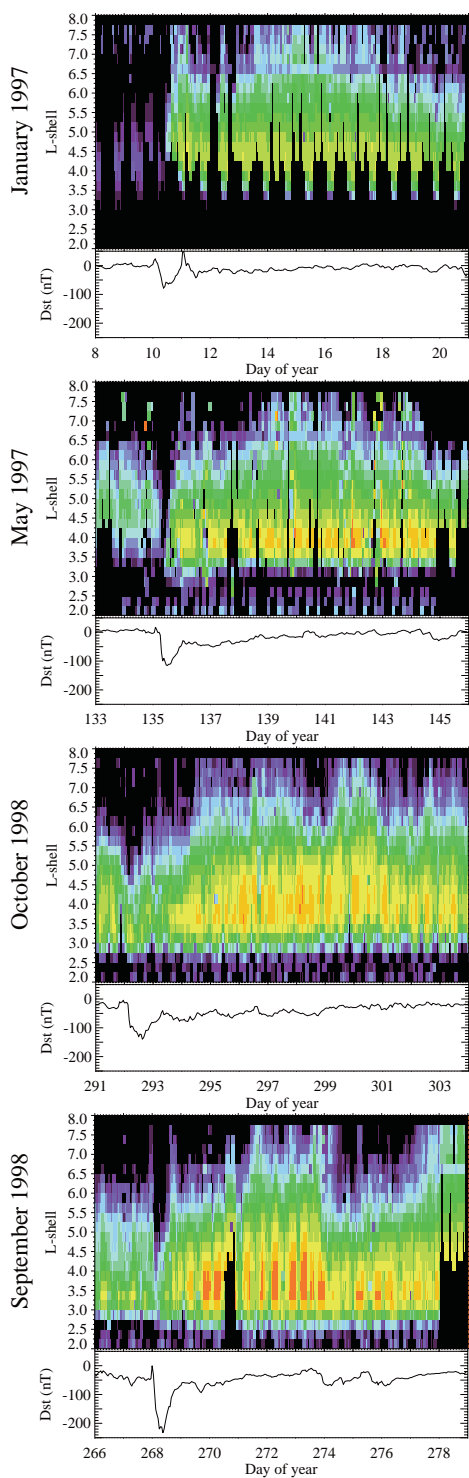


Figure 2  
1-column, print at 100%



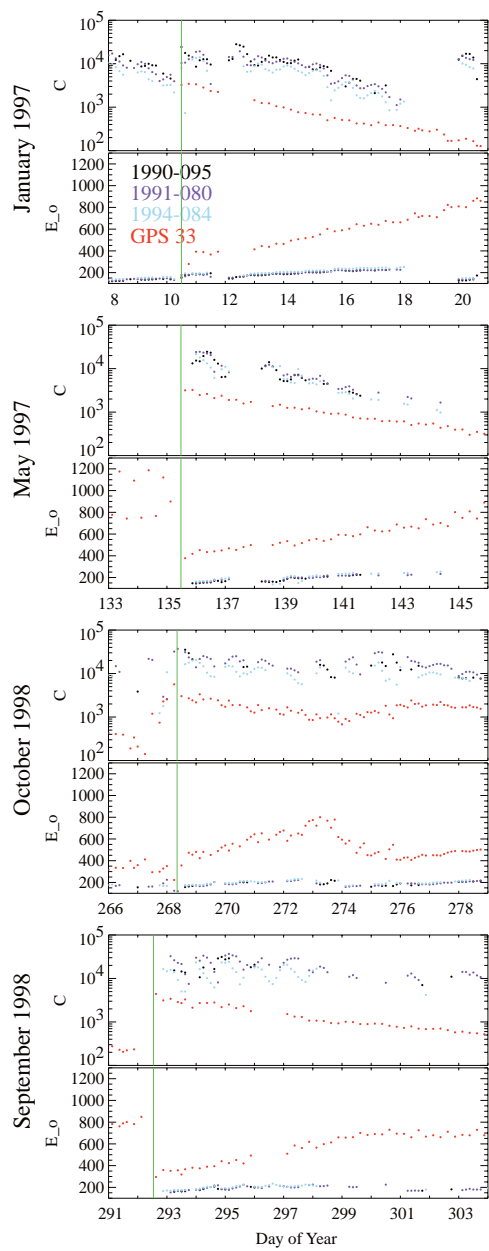


Figure 4  
1-column, print at 100%

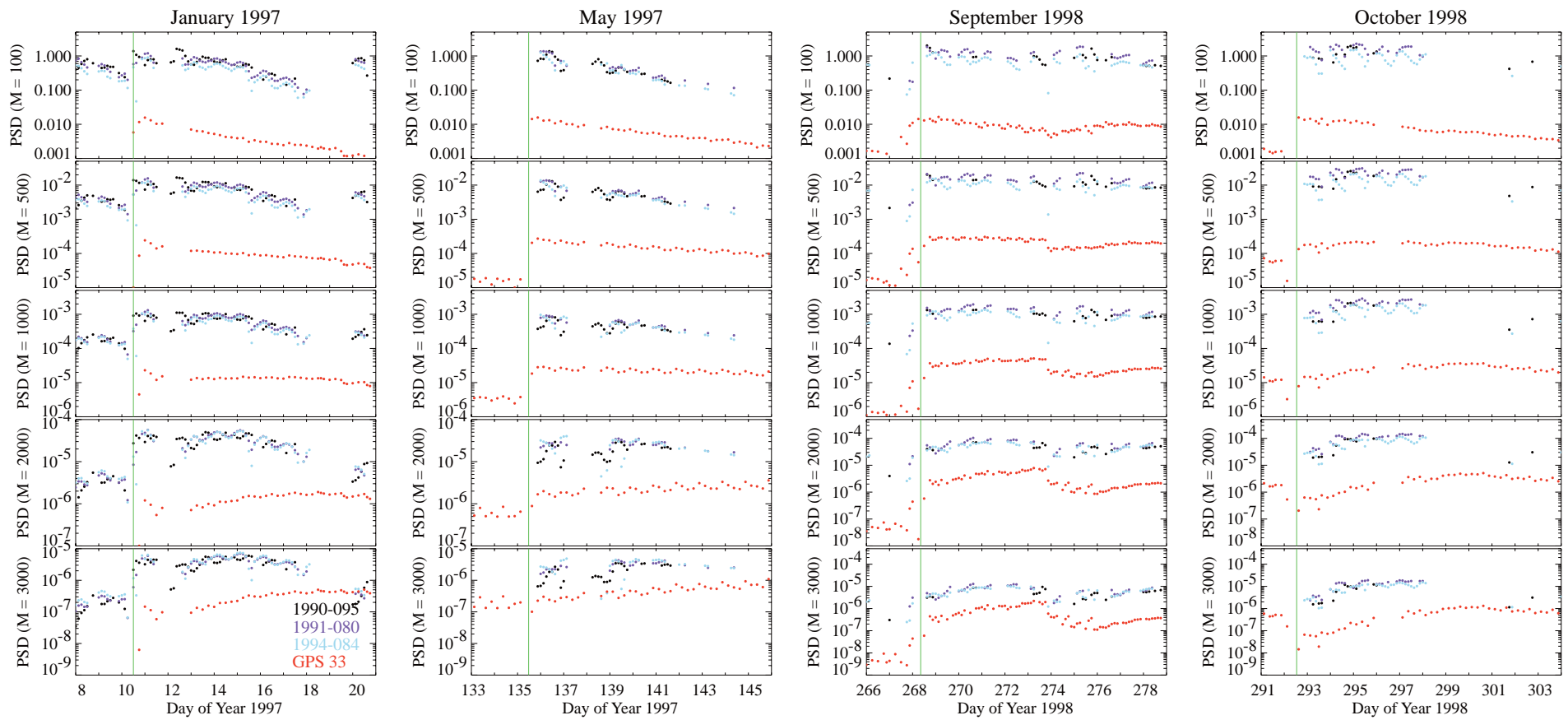


Figure 5  
2-column, print at 66%